sciendo
10.2478/jlecol-2022-0010 Journal of Landscape Ecology (2022), **Vol: 15 / No. 2.**

IMPACT OF LAND USE/LAND COVER CHANGE ON SOIL RETENTION SERVICE:

A CASE OF AGRICULTURAL-URBANIZED LANDSCAPE IN NORTHERN IRAN

MOSTAFA KESHTKAR, ZAHRA MOKHTARI, ROMINA SAYAHNIA*

Environmental Sciences Research Institute, Shahid Beheshti University, Tehran, Iran
**Corresponding author email: r_sayahnia@sbu.ac.ir*

Received: 31st March 2022, **Accepted:** 3rd June 2022

ABSTRACT

Globally, urbanization changes land use/land cover (LULC) and alters ecosystem functions and services. Soil retention (SR) is a critical ecological service that is strongly related to LULC change. The topic of this study is assessment of LULC change on soil retention service (SRS) in a fragile seminatural-urbanized landscape of the Jajrood basin in Northern Tehran, Iran, from 2000 to 2020. To achieve the goal, the LULC maps and the other relevant datasets were imported into the Integrated Valuation of Ecosystem Services and Trade-offs tool (InVEST) using the Universal Soil Loss Equation (USLE). Calibration and validation were performed using Goodness-of-fit test for observational and modeled data. The results revealed that LULC change had both negative and positive effects on SR. The built-up area increased dramatically by about 133 percent, while the rangeland shrunk by approximately 5 % during the twenty-year, leading to an increase in soil erosion and reducing SR. On the other hand, the agricultural and gardening activities expanded by 41 %, which caused an increment in SR. Due to the outgrowth of man-made areas compared to the other land uses, the overall SR decreased by about 17,000 tons. Moreover, the result indicated that slope, elevation, and land management factors, respectively, had the highest correlation with SRS. The finding of this research can provide insight to land use planners to protect the areas with high soil erosion.

Keywords: Ecosystem Service; Universal Soil Loss Equation; InVEST; Land Use Change; Spatial planning, Jajrood Basin.

INTRODUCTION

Land use/ land cover (LULC) alteration significantly changes the ecological circumstances of the earth (Lambin *et al.,* 2003), which consequently affects ecosystem service (Song & Deng, 2017). The Millennium Ecosystem Assessment defined ecosystem service (ES) as 'the benefits that people obtain from ecosystems' which are classified into four categories includes providing, supporting, regulating, and cultural services (MEA, 2005). As a critical regulating service, land soil retention service refers to the function provided by terrestrial ecosystems that control soil erosion (Zhu *et al*., 2019). Soil retention is calculated as potential soil erosion in case of any vegetation cover (maximum erosion) minus actual soil erosion (Zhu *et al.,* 2019). In the other words, vegetation cover prevents the soil from erosion;

considering an indicator of erosion control service that can determine the amount of SR (De Groot *et al.*, 2010). Sediment retention service (SRS) is the capacity of ecosystems to regulate eroded sediment that can settle in streams and provide benefits for soil retention and water quality (Bogdan *et al.*, 2016).

Soil dynamics at the watershed scale are mainly controlled by multiple factors such as climate, rain intensity, soil properties, topography, vegetation, and conservation practices (Gurung *et al.*, 2018; Hamel *et al.*, 2015; Sharp *et al*., 2016). To conserve soil, vegetation is a regulating tool that prevents the soil from erosion and enhances sediment retention, while land use change may reduce vegetation which leads to soil erosion (Abdulkareem *et al.*, 2019; Hamel *et al*., 2015; Srichaichana *et al.*, 2019).

In terms of soil study, the research mainly considers quantifying the amount of soil erosion, however, there is a paucity of research assessing the spatial distribution of SRS (Chen *et al*., 2019). Integrating satellite imagery, remote sensing, and InVEST software can help investigate SRS change and address the gap (Asadolahi *et al*., 2015). InVEST is a geospatial tool for evaluating the impact of LULC change on various ESs (Sharp *et al*., 2016). In terms of SRS estimation, Asadolahi et al. (2017) used InVEST tool to generate an SRS map in the Hyrcanian forest, Iran. In another study, Arunyawat and Shresth (2016) imported the LULC dataset, rainfall, soil characteristics, and topography into the InVEST to extract the SRS in Thailand (Arunyawat & Shrestha, 2016). Bogdan *et al.* (2016) assessed the SRS using various data like LULC map, topographic map, and precipitation in a mountain landscape in Romania. Further, spatial and temporal characteristics of soil conservation services were investigated in the upper and middle areas of the Yellow River, China from 2000 to 2010 (Zhu *et al*., 2019).

Due to a lack of implementation of sustainable land use planning practices, the annual rate of soil erosion in Iran is 33 tons per hectare, which is 6.5 times more than international standards (Hosseini & Ghorbani, 2005). A wide range of on-site and off-site adverse effects of soil erosion causes reduced soil quality (Foley *et al*., 2005); increases the sedimentation in dam reservoirs (Ouyang *et al.*, 2010), and consequently increases water treatment costs (Lal & Research, 2014). Therefore, estimating the amount of soil erosion and accordingly taking appropriate measures is critical in ecosystem protection.

The Jajrood watershed in Northern Iran, as one of the most ecologically valuable and fragile regions, has faced dramatic human development and settlement in recent decades due to its vicinity to Tehran, the capital of Iran (Mirzaei & Hasanian, 2013). Constructing the Latian and Mamlo dams in 1967 and 2000 has amplified the vulnerability of this ecosystem. Furthermore, due to its favorable weather and being away from Tehran's air pollution, this area has become a popular tourism and settlement destination for residents. On the other hand, given the significant contribution of the Latian and Mamlo dams to the water supply of the Tehran metropolis (supplying more than 30 percent), the environmental circumstance of the Jajrood basin and its protection is of great importance (Bidhendi *et al.*, 2008). Considering LULC change and urban expansion in Jajrood, soil erosion poses significant threats to the water reservoirs. Therefore, the purpose of this research is to assess the SRS change that resulted from land use change between 2000–2020. To achieve this goal, climatic data, soil data, digital elevation model (DEM), and LULC maps were imported into Universal Soil Loss Equation (USLE) model.

MATERIALS AND METHODS

Study area

The Jajrood basin is located between the geographical coordination of 51 ° 22 'to 51 ° 51' Eastern longitude and 35 °45 'to 36 ° 50' Northern latitude. Jajrood River, as the main water body of the region, originates from the Kaloon Bastak Mountains and is located in the northeast of Tehran, passes through the Jajrood protected area and the Khojir national park, and eventually reaches the Varamin plain. The highest and lowest elevation in the watershed's northern area is about 4,100 and 1,200 meters. Climatically, this region is categorized in the cold and dry zones with an average precipitation of 280 millimeters.

Notably, as can be seen in Fig. 1 Latian and Mamlo dams are located in this basin. The Latian dam is located 10 km northeast of Tehran and south of Lavasan. This concrete dam provides 30 % of Tehran's drinking water. The Mamlo dam was constructed 30 km southeast of Tehran to supply agricultural and drinking water. To investigate more accurately, the Jajrood basin was categorized into five sub-basins, which are numbered 1, 2, 3, 4, and 5 in Fig 1.

Fig. 1: The geographic location of Jajrood basin and sub-basins

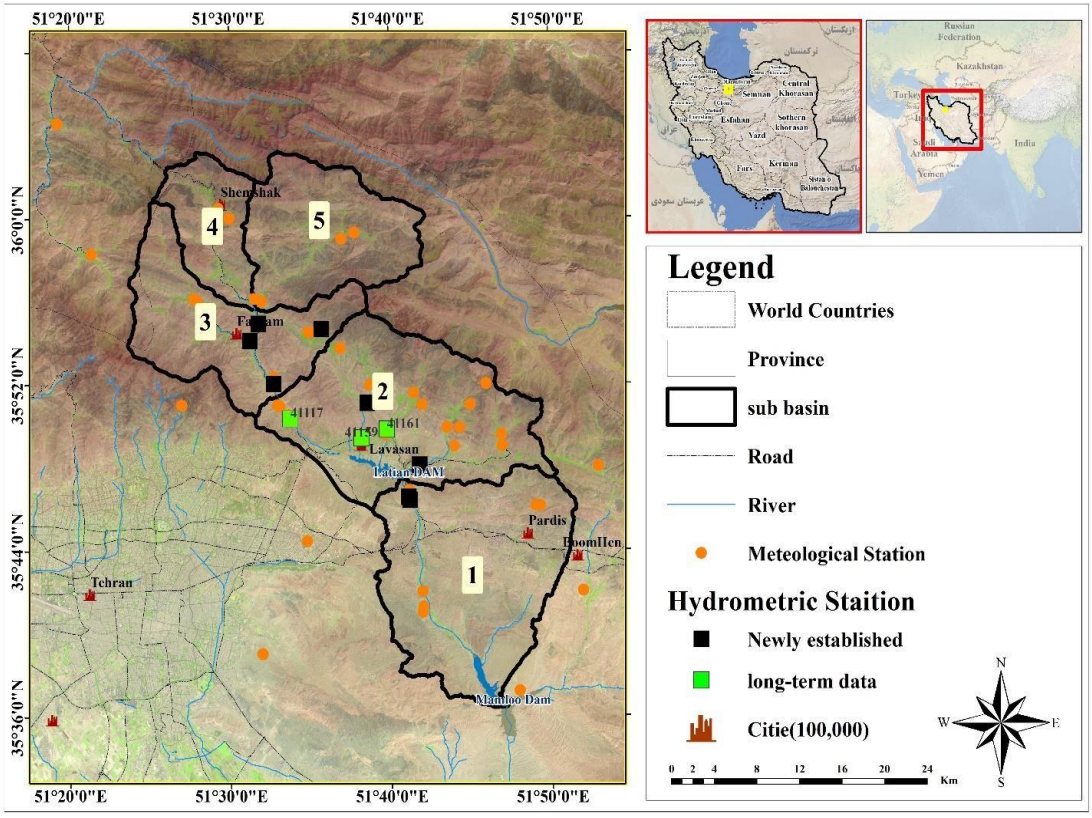

Methodology

Using satellite imagery and remote sensing techniques, the most appropriate method for land use classification was determined among the multiple methods. Fig. 2 demonstrates the

schematic diagram of the research's methodology. Generally, the methodology consisted of two phases: LULC mapping and applying it in estimating SRS along with the other relevant data.

Fig. 2: Research methodology

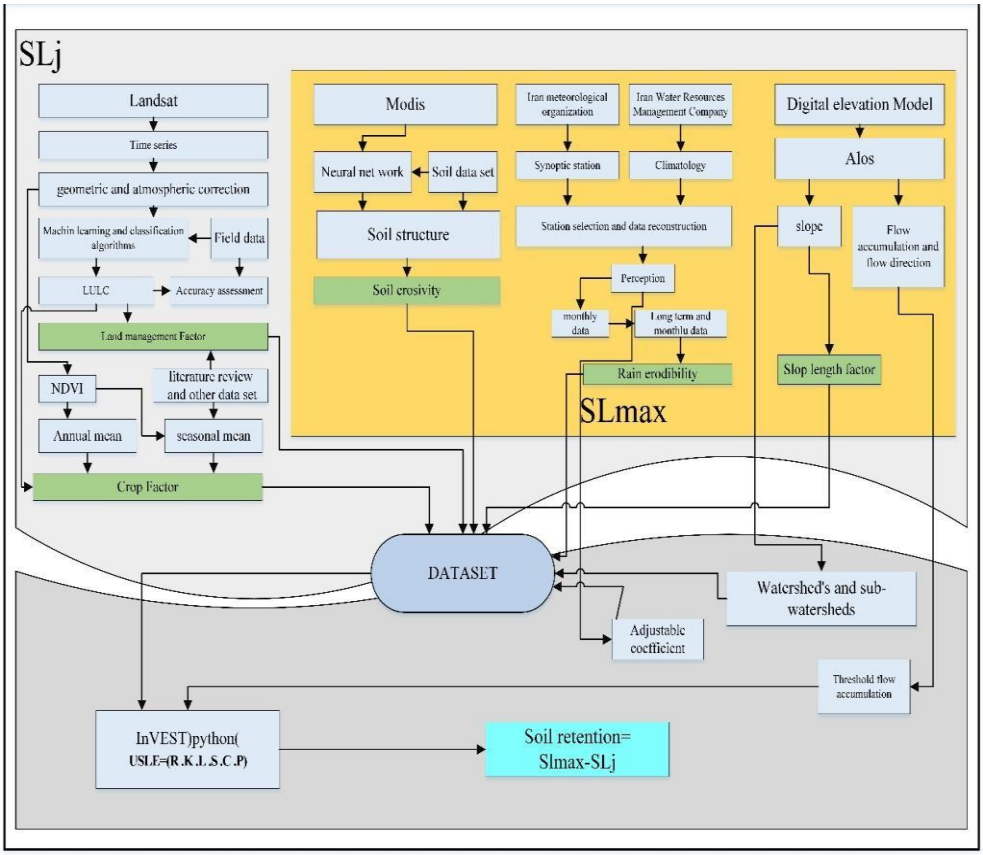

LULC classification

Images of ETM, Landsat 7 and OLI-TIRS Landsat 8 were used to generate LULC (Table 1 - Appendix). After preprocessing the images which included radiometric correction and geocoding, in order to improve the spatial accuracy and resolution, the Pansharp method was conducted and the panchromatic band of the Landsat 7 and 8 were used in TerrSet software. The LULC was categorized into four classes: man-made, vegetation, rangeland, and water (Table 2 - Appendix). Classifying the LULC, the supervised methods included the algorithms of Maxlike, Multi-layer Perceptron (MLP), Fisher, minimum distance (Mindis), and K-Nearest Neighbor (KNN) were used.

The steps taken in the post-processing step included applying filters, merging the classes, removing unnecessary land uses, and finally assessing the accuracy of LULC. Before applying image classification, it is required to estimate the accuracy of the generated maps with ground truth. The most common method for assessing accuracy is to create an error matrix or dummy matrix (Foody, 2002).

This matrix compares cells to cells, and recognizes the cells, or ground truth with their corresponding cells in the classification results. In this study, using the error matrix, the indices like overall accuracy and Kappa coefficient were determined.

In order to compare the LULC accuracy, the producer's accuracy, user's accuracy, omission commission errors were used. Accordingly, the Maxlike algorithm because is considered a highly accurate method and was used to assess change by assessing the SR dynamic over 20 years.

SR estimation

In this study, we used InVEST as a spatially explicit integrated modelling tool and a set of Geographical Information Systems models to quantify and assess spatial-temporal changes in soil erosion potential (Sharp, 2014). Various tools from this package have been used frequently in different case studies to quantify ESs (Asadolahi *et al*., 2017; Zarandian *et al.*, 2017).

The potential of each watershed for soil retention was assessed through a combination of different data sets of LULC, precipitation, soil properties, and topographic conditions (Sharp, 2014; Asadolahi *et al*., 2017; Zhu *et al*., 2019). In this module of InVEST, the universal soil loss 2equation (USLE) (Wischmeier & Smith, 1978) was used, measuring the erosion rate and then calculating the SR rate (Borselli *et al.*, 2008). The SRis affected by five factors as follows:1) rain erosivity, 2) soil erodibility, 3) slope length-gradient, 4) crop factor, and 5) support practices (Sharp *et al.*, 2014). The calculation is based on a ton per hectare per year (ton. ha^{-1}. yr^{-1}) (Renard *et al.*, 2011).

In Equations 1 and 2 (Eq. 1 and 2), SLj and SLmax indicate soil erosion potential and maximum soil erosion, where R, K, LS, C and P stand for the amount of soil loss per given area unit, rainfall erosivity, soil erodibility, slope length-gradient factor, the factor of land cover, and support practice factor respectively.

$$SLj(USLE) = R * K * LS * C * P \quad \text{.....1}$$

$$SLmax = R * K * LS \quad \text{.....2}$$

To estimate SRS, we used Eq.3.

$$\text{Soil } Retention\ Service = SLmax - SLj = R\ K\ LS(1 - CP) \quad \text{.....3}$$

Equation 4 is used to calculate the SR rate:

$$SR\ rate = {}^{SR}/Potential\ soil\ erosion \times 100\% = (1 - CP) \times 100\% \quad \text{.....4}$$

The factors of soil erosion are described below:

Rain erosivity factor

Rain erosivity is defined as the raindrop's potential impact on the erosion rate. In other words, it is the erosion factor in departing and transferring soil particles (Lal, 1998). To calculate the rainfall erosivity factor (R) in this study, the monthly and annual rainfall of 19 precipitation stations in the basin area were collected. The rainfall erosivity factor of the

proposed method was derived by Renard & Freimund (1994). To determine the rainfall erosivity factor, the Fournier index was calculated for all the stations using Eq. 5.

$$F = \frac{\sum_{j=1}^{12} {p_i}^2}{\sum_{j=1}^{12} P} \quad \text{.....5}$$

Where: F is the Fournier index, Pi and P indicate respectively monthly rainfall and annual precipitation (mm).

After determining the Fournier index for the stations using and placing the Fournier index, the amount of R factor for stations was estimated (Renard & Freimund, 1994). The rainfall erosivity unit is *MJ mm ha^{-1} h^{-1} y^{-1}*. Then, using the geostatistical toolbox and the Kriging method, the rainfall erosivity map was depicted in the software GS+ and ArcMap.

R-Factor = $(0.07397 * F^{1.847})/17.2$ F<55mm 6

R-Factor = $(95.77-6.081*F+0.477* F^2)/17.2$ F≥55mm.....7

Soil erodibility factor

We used soil structure information and satellite images and ground datasets to calculate soil erodibility in this study (Hengl *et al*., 2014). The soil erodibility factor is the rate of soil erosion per unit of rainfall erosivity index (Wang, Zheng, Römkens, & Science, 2013). This factor depends on different drivers such as soil texture, soil structure, organic matter, and soil permeability characteristics (Asadolahi *et al*., 2017). The soil erosion factor is estimated based on tons per hectare per hour per hectare mega Joule/ mm (*t. ha.h/ha.MJ.mm*). The soil texture was prepared based on the soil texture triangle method, and then the K factor was calculated based on the soil structure data and soil organic matter content according to Eq.8.

$$\left\{0.2 + 0.3exp[-0.0256S_d]\left(1 - \frac{S_i}{100}\right)\right\} \times \left(\frac{S_i}{CL+S_i}\right)^2 \times \left[1.0 - \frac{0.25C}{c+\exp(3.72-2.95C)}\right] \times \left[1.0 - \frac{0.7SN}{SN+\exp(-5.51+22.0SN)}\right] \quad \text{.....8}$$

Slope length - gradient factor

Regarding the calculation of the slope length - gradient factor (LS factor), L and S factors indicate the effect of topography on soil erosion. Increasing the length and degree of a slope causes rising a flow rate and consequently increases soil erosion. Erosion is more sensitive to slope steepness variation than the slope length (McCool *et al.*, 1989). The L factor is the horizontal distance from the soil flow to the region where the slope is sufficiently reduced to begin the deposition or the distance to the region where the runoff accumulates in a channel. The L factor is calculated by the following equation (Eq.9) (Desmet & Govers, 1997).

$$L_{ij-in} = \frac{\left[\left(A_{ij-in} + D^2\right)^{m+1} - \left(A_{ij-in}\right)^{m+1}\right]}{\left(D^{m+2}\right) \times \left({X_{ij}}^m\right) \times (22.13)^m} \quad \text{.....9}$$

Where:

$L_{ij\text{-}in}$: slope length in i-j cell

$A_{ij\text{-}in:}$ contributing area($m^{2)}$ at the inlet of i-j cell

D: cell size
m: is the length index of the L factor
X_{ij}: $(\sin\alpha_{i,j} + \cos\alpha_{i,j})$ where is the aspect direction for cell i
M: slope factor which is acquired from Eq.10 and 11:

$$M = \frac{\beta}{1+\beta} \quad \ldots\ldots\ldots\ldots\ldots\ldots\ldots\ldots\ldots\ldots\ldots\ldots 10$$

$$\beta = \frac{\sin\theta/0.0896}{0.56+3.0(\sin\theta)^{0.8}} \quad \ldots\ldots\ldots\ldots\ldots\ldots\ldots\ldots\ldots\ldots\ldots\ldots 11$$

θ is the angle of the slope; by increasing the slope gradient coefficient (S), the amount of soil loss increases faster than increasing the slope length. The slope gradient coefficient (S) is the ratio of soil loss in the region to the amount of the soil loss in the slope of 9 % (the standard plot in the USLE model is a length of 22.1 m and a slope of 9 %). S is calculated from the following equation (Eq. 12):

$S = 10.8 \sin\Theta + 0.03 \quad \Theta < 5.14 \ldots\ldots\ldots\ldots\ldots\ldots\ldots 12$

$S = 16.8 \sin\Theta - 0.50 \quad \Theta \geq 5.14$

To estimate the slope-length-gradient factor, we provided the Digital Elevation Model (DEM) of the study site from the Advanced Land Observation Satellite (ALOS) with a resolution of 12.5 meters. Considering the pixel size of the produced land use after mosaicking, the resolution of the images was increased to 15 meters (Fig 3a).

Crop factor

The land cover (Crop) factor is the effect of planting practices and vegetation cover on soil degradation. Vegetation cover on the ground surface reduces soil erosion (Mehri *et al*., 2018; Kouli *et al*., 2009). In this study, to calculate C in the Jajrood basin, a normalized difference vegetation index (NDVI) was used (Kouli *et al*., 2009) as follows in Eq.13 and 14:

$NDVI = (NIR-R)/(NIR+R) \quad \ldots\ldots\ldots\ldots\ldots\ldots\ldots\ldots\ldots 13$

$C = (1-NDVI)/2 \quad \ldots\ldots\ldots\ldots\ldots\ldots\ldots\ldots\ldots\ldots\ldots\ldots 14$

Management factor

The amount of support (conservation) factor (P factor) depends on the watershed management and land support practices as well as the plowing of the soil (Alizadeh, 2014; Mehri *et al*., 2018). In this study, the amount of support factor was calculated using LULC classification (Deore, 2010; Wischmeier & Smith, 1978). This index is considered a support operation that is implemented on LULC.

Validation and calibration

To calibrate the model, the simulated annual average was compared to the observed annual average sediment using the Sediment Delivery Ratio (SDR) INVEST model. The computation of the connectivity index (CI) for each pixel was used to estimate SDR as a function of the upslope area (Ud) and downslope flow path (Dd) to the streams based on

DEM (Borselli *et al*., 2008), which determines the degree of hydrological connectivity of a pixel/area/to the stream. The SDR for a pixel i was directly derived from CI using a sigmoid function (Vigiak *et al*., 2012 (Eq.15).

$$SDR_i = {SDR_{Max}}\Big/{1 + exp\left(\frac{IC_0 + IC_i}{K_b}\right)} \quad \text{……..15}$$

The Borselli k (kb) and Borselli ICo (ICo and ICi) parameters are calibration parameters that define the shape of the SDR-IC relationship (Sharp *et al.*, 2016). The default value for each parameter is set and reduced or increased for calibration (Hamel *et al*., 2015; Vigiak *et al*., 2012). Therefore, sediment load or export from given pixel i, Ei *(t/ha/yr)* is calculated using Eq.16.

$$E_i = USLE_i \times SDR \quad \text{……..……..……16}$$

Where, SDR is the sediment delivery ratio for pixel i which is the proportion of fine sediment produced in a given area that travels with the overland flow and waterways (Hamel *et al.*, 2015; Sharp *et al*., 2016). The total sediment export /load *(t/ha/ yr)* in sub-basins is calculated by Eq. 17.

$$E = \sum_{i=0}^{n} E_i \quad \text{……..……17}$$

Where E_i is sediment export/load.

Data sets related to eleven hydrometric stations of the study area were (Fig. 1) used to calibrate the model. The parameter IC, flow accumulation, K, and observed data (long-term SDR from 2000 to 2018) collected from three hydrological stations (From 11 available stations) were used to calibrate the SDR. The value of parameters varied until the error became minimized (the error was defined as the difference between the estimated and observed sediment). The calibration period of each hydrographic sub-basin depended on the availability of observed data from hydrometric stations (Table 3 - Appendix). The unit for the observed data were mg per litre *(mg/l)*, while the unit of the estimated data were ton per year *(ton/year)*. Accordingly, the observed data were transformed to ton/year using Eq.18 for all stations.

$$SC = b \times Q^c \quad \text{…….18}$$

Where SC *(t/day)* sediment loss, Q is streamflow rate *(m^3/s)*, b and c are constants, which are determined from the sediment concentration (*g/ml*) and streamflow. Some of the metrological data (approximately 10 %) were missed which was solved by taking the mean value of near stations (Ferrari & Ozaki, 2014).

In the hydrographic sub-basins, the diversion of water flow by dam systems was Not additionally considered. The calibrated parameter values were used to obtain each station basin under the assumption that the calibrated value captured the climate characteristics, land use, and topography of the basins.

In order to test the applicability and reliability of the applied models, a comparison of simulated results against the observed data is necessary. In this research, we used R2 and PBIAS. When PBIAS shows a low absolute value, then the model has better performance. If

the R2 value is N0.75 and PBIAS is b ± 10 %, then the model has a very good performance. If the R2 is b0.50 and PBIAS is N25 % then the model is unsatisfactory and not applicable (Moriasi *et al*., 2007; Munoth & Goyal, 2019).

RESULTS

LULC Change

Table 4 (Appendix) shows the results of the overall accuracy and Kapa coefficient for different methods and various cell sizes. By comparing the results, it becomes evident that the highest accuracy belongs to the Maxlike which was selected as the proper algorithm in this study. Table 5 (Appendix) represents the accuracy and errors for 15- and 30-meters cells. We used the 15-meter pixel size to compare the accuracy of each class in the Maxlike method. After classification, the area of each class was calculated. As shown in Table 6 (Appendix), the rangeland class shrunk by 5 percent from 2000 to 2020. In contrast, man-made and vegetation land use increased by 57 and 29 percent. Due to the population growth and water availability, agricultural and gardening activities became popular and led to the rise in vegetation cover. The water area also expanded by 55 percent due to the Mamlo dam construction and its dewatering in 2000. Table 7 (Appendix) indicates how land use changed during the 20-year and a substantial area of the rangeland was converted into the man-made and residential classes. Fig. 3 and 4 show the final LULC classification in 2000 and 2020 and its change over time. It is clear from the maps that the highest man-made development occurred in sub-basins 1 and 2 as they possess favourable topography for human activities and are close to the dams.

Fig. 3: Land use classification in 2000 and 2020

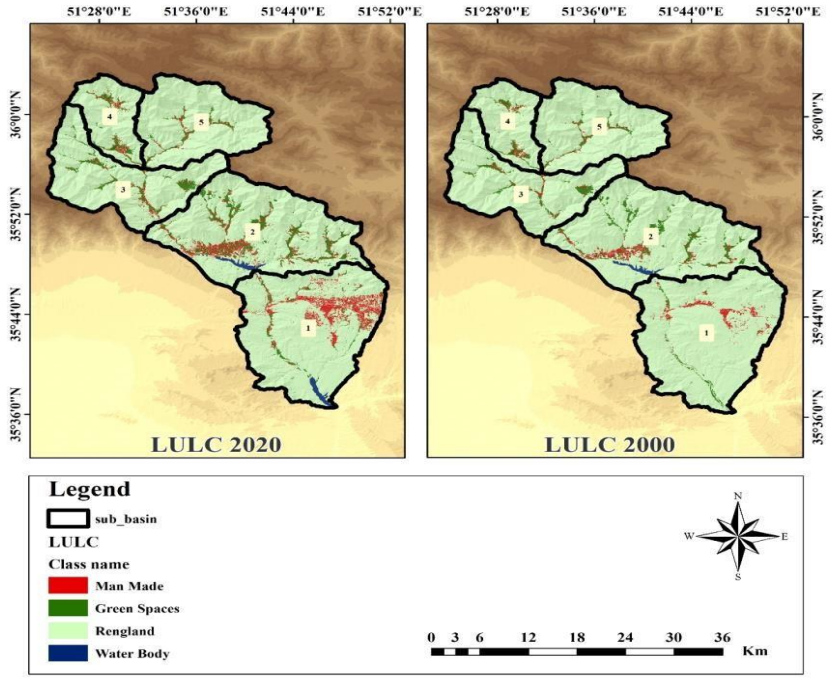

Fig. 4: Land use change between 2000 –2020

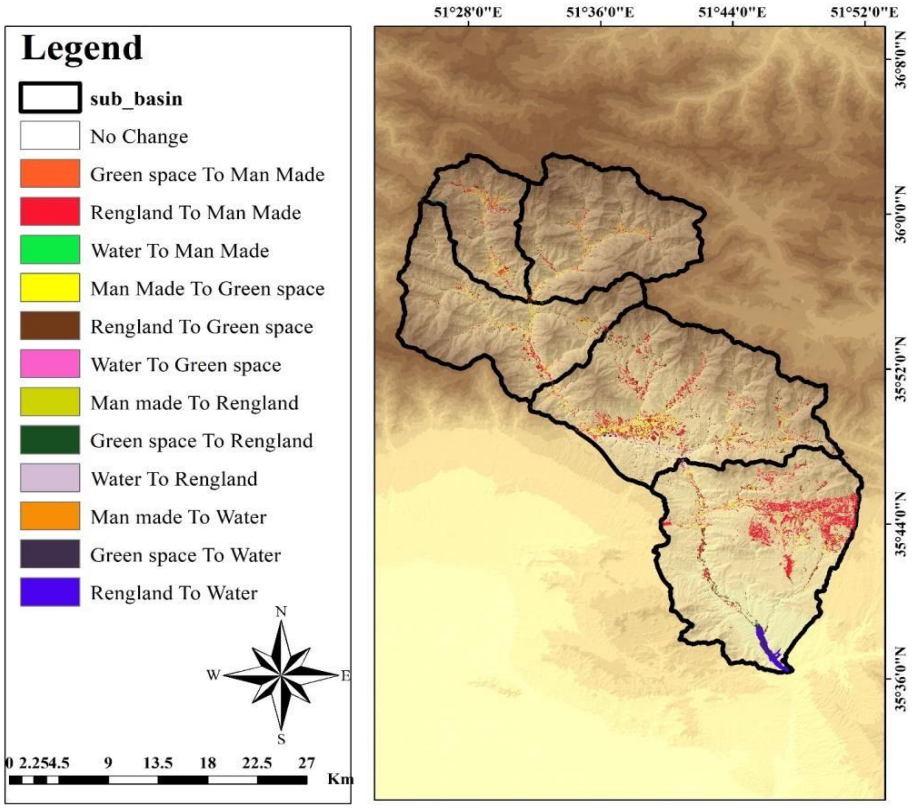

Validation and calibration of the model

Validation and calibration of the InVEST SDR model was undertaken by comparing the annual simulated data against observed data. These observed data, were obtained from the Iran Water Resources Management Company (WRM). The performance of the model was checked using the Coefficient of Determination (R2) and Average Percentage Bias Error (PBIAS) (Gyamfi, 2016; Munoth & Goyal, 2019). The predicted soil loss and sediment export were consistent with the corresponding estimates from the observed data over a period. This indicates the suitability of the SDR model for simulating the sediment loss and sediment export of the Jajrood watershed. The observed average annual sediment loss at four stations is presented in Fig.5 These results were consistent with the results obtained using the model.

The mean value of observed and simulated sediment loss for ST41-117 in calibration was 319.75 and 318.81 thousand tons/year, respectively. The low discrepancy (R2= 0.87) of sediment loss suggests that LU/LC effects have been sufficiently estimated by the model. The R2 and PBIAS values were applied to check the performance of the SDR model for each station over 20-years (Fig. 5). The results indicated the suitability of the InVEST SDR model for modeling sediment export in the Jajrood watershed.

Fig. 5: Validation of model performance in each station from 2000 to 2019

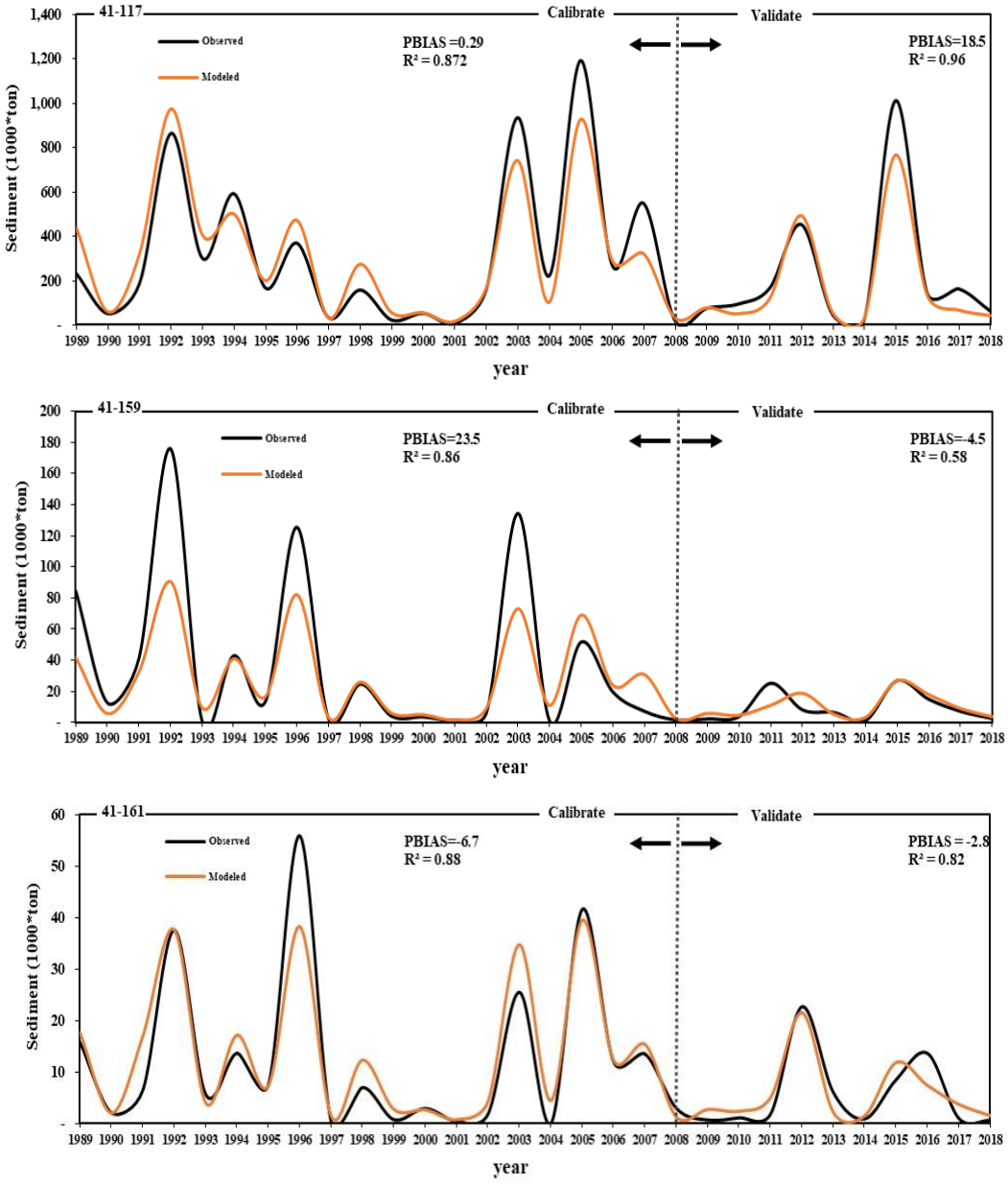

Soil retention service (SRS) change

As shown in Fig. 6, the rain erosivity varied between 43.6 and 1908.1 across the basin, with an average of 708.8 MJmmha -1h-1 y-1 and a standard deviation of 448.5. It should be noted that the highest rainfall erosivity occurred in the mountainous regions in the north, and the least has been witnessed in the southern parts. Soil erodibility values were calculated based

on the soil structure. This value varied between 0.061 and 0.0778 Mg ha ha-1 MJ-1 mm-1 in the SI unit. Fig. 6 illustrates the spatial distribution of soil erodibility in the study area. The slope length was calculated using Eq.9. In the mountainous region (northern part), the slope length is higher than in the plain area. In the study area, this factor varied substantially across the region. The management factors or C and P factors were estimated based on the land use. This is the critical parameter in monitoring the SRS. The results revealed that this parameter increased during the time in valleys due to planting trees and gardening.

After providing the required data, including rainfall erosivity, soil erodibility, land use, and digital elevation model, IC, and K indices, they were introduced to the InVEST3.4.0. Accordingly, the maximum soil loss potential (SLMAX) considering three factors of R, K, and LS for 2000 and 2020 showed that its range varied from 0 to 90 tons per hectare and the average was 0.95 tons per hectare (Fig. 7).

As mentioned before, human development increased substantially in sub-basin 1 compared to the other ones. In the same way, the agricultural land and garden also expanded in this sub-basin. It can be seen in table 8 (Appendix) that sub-basin 3 and 5 experienced the maximum soil erosion. Generally, the soil erosion in all sub-basins increased during the 20 years. The erosion increased in sub-basin 1 by 5.5 percent. It was estimated that 17,000 tons of soil was eroded and soil erosion increased by 0.68 percent from 2000 to 2020. Furthermore, the ratio of soil erosion to the total area of the basin rose in the given period. In addition, we estimated the soil erosion for each LULC class, which was decreased by about 44,000 hectares/ton in the rangeland class. In contrast, it was increased in man-made, vegetation, and water classes (Table 9 - Appendix).

Fig. 6: Spatial distribution of the(a) rain erosivity(b) soil erodibility(c) slope-length (d) C and P factors

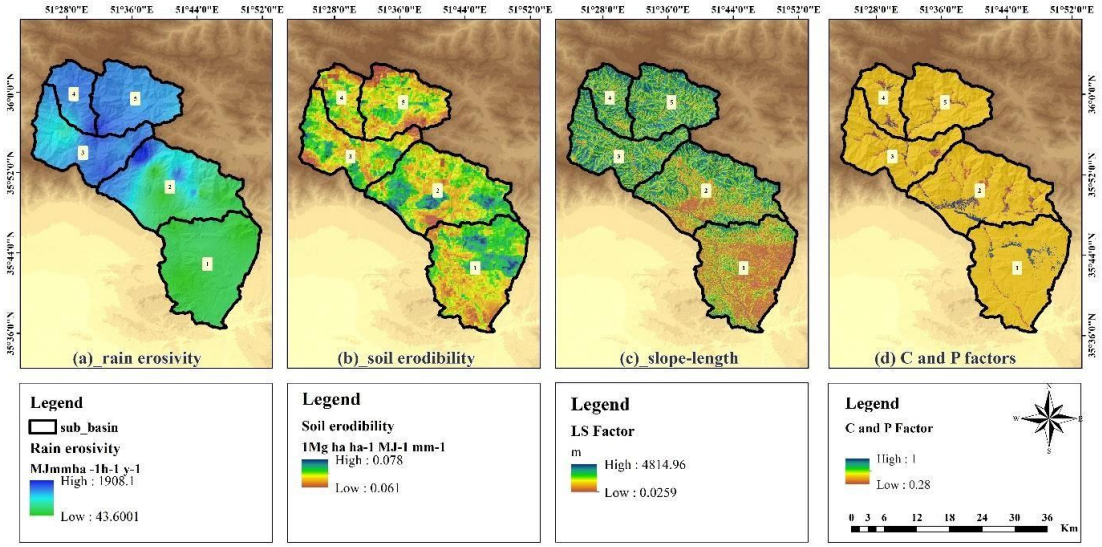

Fig. 7: (a) Maximum soil erosion(b) soil erosion in sub-basins in 2000 (c) and soil erosion in sub-basins in 2020

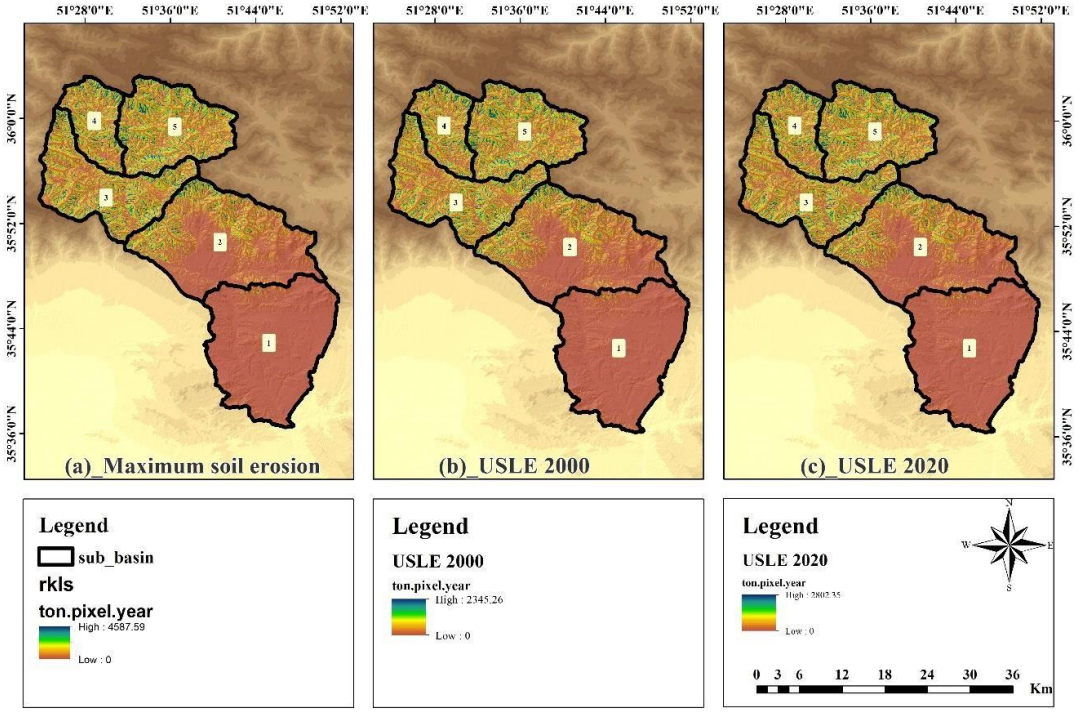

According to the results, SR potential using the SLmax-SLJ equation for 2000 and 2020 were 0.778 and 0.776 tons per hectare per year. The minimum and the maximum SR in 2000 and 2020 varied from 0 to 61.9 tons/hectare. Our results in table 10 (Appendix) represent that the potential SR decreased in all sub-basins during the given period (Fig 8.). The SR increased moving from downstream to upstream due to the unfavorable topographic conditions for human activities. Rangeland degradation induced SRS experienced a reduction in this time interval; however, in the other classes, the service increased (Table 11 - Appendix). The results of the correlation between the generated data and SR according to Table 12 (Appendix) represent that the slope, elevation, and land management factors have the highest correlation with SR. Rain erosivity and soil erodibility were also correlated with SR. However, this correlation was less significant than the other factors, which indicated the lower role of these two factors in soil erosion.

Fig. 8: Soil retention service in 2000 and 2020

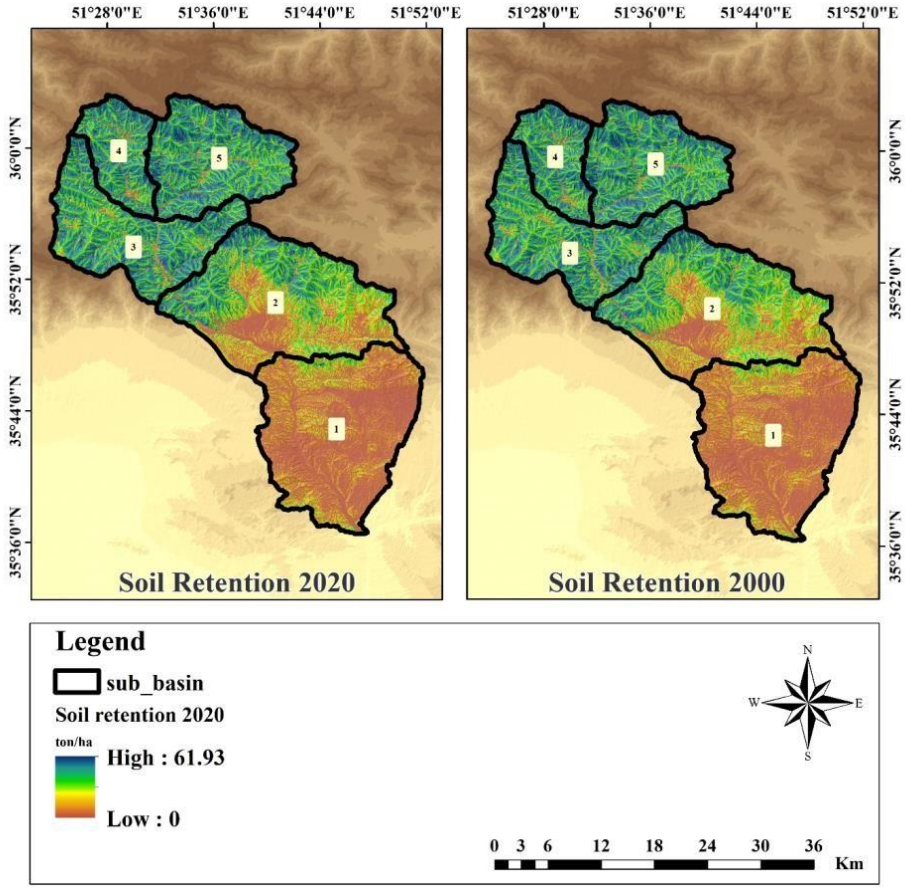

The results demonstrated that the region experienced developments over the past 20 years. In addition to the human developments, the vegetation cover has increased as well. On the other hand, the average SR rate has decreased, but by increasing vegetation cover, the potential SR has risen by 0.2 tons per pixel per hectare. The mountain parts of the basin in the north with a high elevation and steep slopes were prone to erosion because of poor vegetation cover and higher precipitation rates. However, the presence of forests and gardens in the valleys led to less erosion and consequently increased SR.

Fig. 9 illustrates that the rate of SR depends on the LULC, slope, and topography of the basin. The vegetation class had the highest amount of SR and the most minor occurrence in built-up areas and water (less than 10 %). The average of this rate was 58 and 47.6 percent respectively in 2000 and 2020. Considering the sub-basins, the highest amount of SR was seen in sub-basin 5, 3, and 4, which was associated with LULC and slope.

Fig. 9: Soil retention rate distribution in the study area in 2000 and 2020

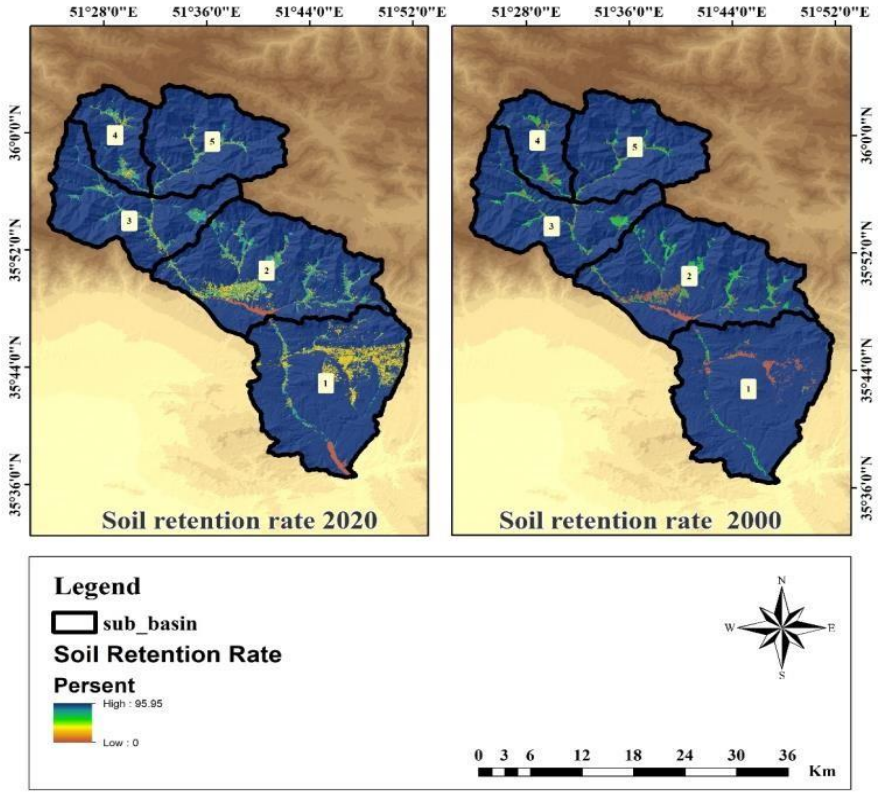

DISCUSSION

Soil loss rate, in Iran, ranged from 3 to12 *t/ha/ year* (Alizadeh, 2014), however, in this study the average soil erosion was approximately 17.05 *t/ha/year* for the entire sub-basin, 43 *t/ha/year* for cultivated land, and a maximum soil loss rate recorded at 186.66 *t/ha/year*. This is associated with the conversion of natural vegetation into urban and cultivated land.

Methodologically, in this study, we emphasized the accuracy of the LULC mapping in SRS assessment. So, several algorithms were applied to ensure the provision of the most accurate algorithm. We used the ground truth points to determine the Kappa coefficient and overall accuracy. Maxlike method with a 15-meter cell size was identified as the most accurate classification method. To assess the soil retention, we applied quantitative spatial analysis of the SRS through the USLE model and geographic information system by importing various datasets to the InVEST model. Zhu *et al*. (2019) applied the USLE-based model to quantify soil conservation in Yellow River, China. Uddin *et al.* (2016) estimated the soil retention dynamic used the USLE-based method to assess the spat distribution of erosion risk across the entire area of the Koshi basin (Uddin *et al*., 2016).

The response to the LULC change across the basin varied substantially due to heterogeneous environmental factors like topography, precipitation rate, and human activities. In some parts of the basin, LULC change derived adverse effects, while in the other

sub-basins, its change had positive impacts. The SR increased from downstream to upstream due to the unfavourable topographic conditions for human activities. For instance, tree planting and gardening in the southern valleys increased soil retention. However, the man-made development in the northern part of the basin could not significantly change soil erosion because of the steep terrain. The LULC change in the whole basin increased soil erosion risks during the past 20 years.

Ecosystem services are closely related to land-use change. Therefore, studies that integrate these components are imperative in the context of land use planning and can ensure the sustainable provision of ESs. Comparing the results with the previous research, LULC change in the middle and upper of the Yellow River altered the amount of soil retention from 2000 to 2010 (Zhu *et al.*, 2019). Fu *et al.* (2011) indicated that the increase in vegetation cover influenced the soil erosion control service in the Loess Plateau, China from 2000 to 2008. Similarly, a study in Europe revealed that deforestation and agricultural practices affected soil erosion and sediment (Bakker *et al*., 2008).

Downstream effects of sediment exported from the basin may pose a major threat to siltation for the hydropower dams in the study area. Such threats are also reported in other parts of Iran, suggesting that accelerated soil erosion in the sub-basin resulted in the siltation of dams (Karki *et al*., 2018).

CONCLUSION

In the present research, we conducted a case study in the Jajrood basin, northern Iran, to assess the effect of LULC change on soil retention as an ecosystem service from 2000 to 2020. Overall, our results indicated that reducing rangeland and expansion in man-made areas has led to increasing soil erosion and decreasing SRS. The findings indicated that human activities like urbanization, agricultural practices, and dam construction changed the LULC over the last 20 years, leading to alteration of soil erosion potential and consequently affecting soil retention service. We recommended future research to determine priority areas for conservation over the basin through multi-criteria decision-making. In addition, to enhance soil management practices, complementary research like was recommended to investigate the spatial distribution of other ESs, analyse trade-offs between multiple ESs, and integrate analysis of various ESs in the Jajrood basin.

ACKNOWLEDGMENTS

The authors are grateful to the editors and anonymous reviewers for providing constructive comments, which are helpful for the improvement of our paper.

CONFLICTS OF INTEREST

The authors declare no conflict of interest.

AUTHORS' CONTRIBUTIONS

MK analyzed and interpreted the data and drafted the manuscript, RS designed the experiment and supervised the research and took part in revising and editing the manuscript and ZM took part in analyses and writing the manuscript.

REFERENCES

Abdulkareem, J., Pradhan, B., Sulaiman, W., & Jamil, N. J. G. F. (2019). Prediction of spatial soil loss impacted by long-term land-use/land-cover change in a tropical watershed. *Geoscience Frontiers 10*(2), 389-403.

Arunyawat, S., & Shrestha, R. P. J. S. (2016). Assessing land use change and its impact on ecosystem services in Northern Thailand. *Sustainability 8*(8), 768.

Asadolahi, Z., Salmanmahiny, A., & Sakieh, Y. J. E. E. S. (2017). Hyrcanian forests conservation based on ecosystem services approach. *Environmental Earth Sciences 76*(10), 1-18.

Bakker, M. M., Govers, G., van Doorn, A., Quetier, F., Chouvardas, D., & Rounsevell, M. J. G. (2008). The response of soil erosion and sediment export to land-use change in four areas of Europe: *The importance of landscape pattern. Geomorphology 98*(3-4), 213-226.

Bidhendi, G. N., Nasrabadi, T., Vaghefi, H. R. S., Hoveidi, H., & Jafari, H. R. J. J. o. e. h. (2008). Role of water-saving devices in reducing urban water consumption in the mega-city of Tehran, case study: a residential complex. *Journal of Environmental Health 70*(8), 44-47.

Bogdan, S.-M., Pătru-Stupariu, I., & Zaharia, L. J. P. E. S. (2016). The assessment of regulatory ecosystem services: the case of the sediment retention service in a mountain landscape in the Southern Romanian Carpathians. *Procedia Environmental Sciences 32*, 12-27.

Borselli, L., Cassi, P., & Torri, D. J. C. (2008). Prolegomena to sediment and flow connectivity in the landscape: a GIS and field numerical assessment. *CATENA 75*(3), 268-277.

Chen, J., Xiao, H., Li, Z., Liu, C., Wang, D., Wang, L., & Tang, C. J. E. e. (2019). Threshold effects of vegetation coverage on soil erosion control in small watersheds of the red soil hilly region in China. *Ecological Engineering 132*, 109-114.

De Groot, R. S., Alkemade, R., Braat, L., Hein, L., & Willemen, L. J. E. c. (2010). Challenges in integrating the concept of ecosystem services and values in landscape planning, management and decision making. *Ecological Complexity 7*(3), 260-272.

Deore, S. J. (2010). Prioritization of micro_watersheds of upper Bhama basin on the basis of soil erosion risk using remote sensing and GIS technology. *International Journal of Water Resources and Environmental Engineering* Vol. 2(3), pp. 130-136,

Desmet, P., & Govers, G. J. I. J. o. G. I. S. (1997). Comment on'Modelling topographic potential for erosion and deposition using GIS'. *International Journal of Geographical Information Science 11*(6), 603-610.

Ferrari, G. T., & Ozaki, V. J. R. B. d. M. (2014). Missing data imputation of climate datasets: Implications to modeling extreme drought events. *Revista Brasileira de Meteorologia 29*(1), 21-28.

Fu, B., Liu, Y., Lü, Y., He, C., Zeng, Y., & Wu, B. (2011). Assessing the soil erosion control service of ecosystems change in the Loess Plateau of China. *Ecological Complexity*, 8, 284-293.

Foody, G. M. (2002) Status of land cover classification accuracy assessment. *Remote sensing of environment*, 80 (1): 185-201 .

Gurung, S. B., Geronimo, F. K., Hong, J., & Kim, L.-H. J. C. (2018). Application of indices to evaluate LID facilities for sediment and heavy metal removal. *Chemosphere 206*, 693-700.

Gyamfi, C., Ndambuki, J. M., & Salim, R. W. J. W. (2016). Hydrological responses to land use/cover changes in the Olifants Basin, South Africa. *Water 8*(12), 588.

Hamel, P., Chaplin-Kramer, R., Sim, S., & Mueller, C. J. S. o. t. T. E. (2015). *A new approach to modeling the sediment retention service (InVEST 3.0):* Case study of the Cape Fear catchment, North Carolina, USA. *524*, 166-177.

Hengl, T., de Jesus, J. M., MacMillan, R. A., Batjes, N. H., Heuvelink, G. B., Ribeiro, E., . . . Walsh, M. G. J. P. o. (2014). SoilGrids1km—global soil information based on automated mapping. *PLoS One 9*(8), e105992.

Hoseini S., Ghorbani, M, Economic of soil erosion. (2005). Ferdousi University Publication. Karki, S., Thandar, A. M., Uddin, K., Tun, S., Aye, W. M., Aryal, K., . . . Chettri, N. J. E. S. R. (2018). Impact of land use land cover change on ecosystem services: a comparative analysis on observed data and people's perception in Inle Lake, Myanmar. *Environmental Systems Research 7*(1), 1-15.

Kouli, M., Soupios, P., & Vallianatos, F. J. E. g. (2009). Soil erosion prediction using the revised universal soil loss equation (RUSLE) in a GIS framework, Chania, Northwestern Crete, Greece. *Environmental Geology 57*(3), 483-497.

Lal, R. J. I. S., & Research, W. C. (2014). Soil conservation and ecosystem services. *International Soil and Water Conservation Research 2*(3), 36-47.

Lambin, E. F., Geist, H. J., Lepers, E. J. A. r. o. e., & resources. (2003). Dynamics of land-use and land-cover change in tropical regions. *Annual Review of Environment and Resources 28*(1), 205-241.

McCool, D. K., Foster, G. R., Mutchler, C., & Meyer, L. J. T. o. t. A. (1989). Revised slope length factor for the Universal Soil Loss Equation. *ASAE 32*(5), 1571-1576.

Mirzaei, M., & Hasanian, H. (2013). *Quality Evaluation of Jajrood River (IRAN) by Quality Indices Methods.* Paper presented at the Advanced Materials Research.

Moriasi, D. N., Arnold, J. G., Van Liew, M. W., Bingner, R. L., Harmel, R. D., & Veith, T. L. J. T. o. t. A. (2007). Model evaluation guidelines for systematic quantification of accuracy in watershed simulations. *ASABE 50*(3), 885-900.

Munoth, P., & Goyal, R. J. W. R. M. (2019). Effects of DEM source, spatial resolution and drainage area threshold values on hydrological modeling. *Water Resources Management 33*(9), 3303-3319.

Ouyang, W., Hao, F., Skidmore, A. K., & Toxopeus, A. J. S. o. t. T. E. (2010). Soil erosion and sediment yield and their relationships with vegetation cover in upper stream of the Yellow River. *Science of The Total Environment 409*(2), 396-403.

Reid, W.V (2005) *Millennium Ecosystem Assessment. Ecosystems and human well-being: Synthesis*. Washington, DC: Island Press; 2005, p. 155.

Renard, K. G., & Freimund, J. R. J. J. o. h. (1994). Using monthly precipitation data to estimate the R-factor in the revised USLE. *Journal of Hydrology 157*(1-4), 287-306.

Sharp, R., Tallis, H., Ricketts, T., Guerry, A., Wood, S., Chaplin-Kramer, R., . . . Olwero, N. J. T. N. C. (2014). *InVEST user's guide*. The natural capital project.

Song, W., & Deng, X. J. S. o. t. T. E. (2017). Land-use/land-cover change and ecosystem service provision in China. *Science of the Total Environment 576*, 705-719.

Srichaichana, J., Trisurat, Y., & Ongsomwang, S. J. S. (2019). Land use and land cover scenarios for optimum water yield and sediment retention ecosystem services in Klong U-Tapao Watershed, Songkhla, Thailand. *Sustainability 11*(10), 2895.

Uddin, K., Murthy, M., Wahid, S. M., & Matin, M. A. J. P. o. (2016). Estimation of soil erosion dynamics in the Koshi basin using GIS and remote sensing to assess priority areas for conservation. *PlosOne 11*(3), e0150494.

Vigiak, O., Borselli, L., Newham, L., McInnes, J., & Roberts, A. J. G. (2012). Comparison of conceptual landscape metrics to define hillslope-scale sediment delivery ratio. *Geomorphology 138*(1), 74-88.

Wang, B., Zheng, F., Römkens, M. J. J. A. A. S., Section B–Soil, & Science, P. (2013). Comparison of soil erodibility factors in USLE, RUSLE2, EPIC and Dg models based on a Chinese soil erodibility database. *Section B–Soil & Plant Science 63*(1), 69-79.

Wischmeier, W. H., & Smith, D. D. (1978). *Predicting rainfall erosion losses: a guide to conservation planning*: Department of Agriculture, Science and Education Administration.

Zhu, M., He, W., Zhang, Q., Xiong, Y., Tan, S., & He, H. J. H. (2019). Spatial and temporal characteristics of soil conservation service in the area of the upper and middle of the Yellow River, China. *Heliyon 5*(12), e02985.

APPENDIX

Table 1: Satellite images in the study

Satellite	Date	Sensor	Path	Row	Resolution
Landsat 7	18/05/2000	ETM	134	35	30
Landsat 8	01/05/2020	OLI/TIRS	134	35	30

Table 2: Land use classification

Land use classes	Description
Man-made	Urban and rural areas
Vegetation	Forests, gardens, and agricultural land
Rangeland	Sparse to massive rangelands
Water	Dams and rivers

Table 3: Information on hydrometric stations and calibration period for the SDR

Station code		Hydrometric station	river	Area(km2)	exposition	Avg. sediment(million ton)	Avg. elevation
41161		Naroon	Afje	30	1989-2018	0.01	1750
41159		Najarkala	Kondrood	59		0.029	1700
41117		Roodak	Jajrood	37		0.29	1890

Table 4: Results of the accuracy assessment in different classification methods

		Classification Methods									
		Maxlike		**Fisher**		**KNN**		**Mindis**		**MLP**	
	Cell size	Overall accuracy	Kapa coefficient	Overall accuracy	Kapa coefficient	Overall accuracy	Kapa coefficient	Overall accuracy	Kapa coefficient	Overall accuracy	Kapa coefficient
Land use (2000)	30	96	96	93.9	89.7	78.7	68	78.62	65.6	93.22	89
	15	96	93.4	93.25	88.5	77.8	66.7	79.4	66.8	89.5	83.4
Land use (2020)	30	87.3	85.01	85.1	83.1	75.4	76.7	82.3	81.54	96.4	94.2
	15	88.7	90.12	91.46	89.3	77	71.2	83.5	81.8	97.4	96.2

Table 5: Error coefficient for land use (2000) using the Maxlike method

	LULC (Maxlike) with cell size 30				LULC (Maxlike) with cell size 15			
Land use classes	**User's Accuracy**	**Commission error**	**Producer's Accuracy**	**Omission error**	**User's Accuracy**	**Commission error**	**Producer's Accuracy**	**Omission error**
Human made	87.8	0.12	90.3	0.096	88.48	0.11	89.2	0.1
Vegetation	97.3	0.02	96.5	0.034	97.3	0.026	96.9	0.031
Rangeland	97.8	0.022	97.15	0.028	97.5	0.0247	97.4	0.0256
Water	1	0	95.4	0.045	1	0	98.5	0.015

Table 6: Contribution of each land use class in 2000 and 2020 and their change between 2000-2020

Land use classes	**Year**				**Land use change**	
	2000		**2020**			
	hectare	**percent**	**hectare**	**percent**	**hectare**	**percent**
Man-made	1991	2.02	4636.64	4.7	2645.64	57.06
Vegetation	3544	3.59	5023	5.09	1479	29.44
Rangeland	92801	94.1	88324.6	89.56	-4476.4	-5.07
Water	285.75	0.29	637.3	0.65	351.55	55.16

Table 7: Land use change matrix for different classes in 2000 and 2020

		2020			
	Land use classes	**Man made**	**Vegetation**	**Rangeland**	**Water**
2000	**Man made**	1130.4	532	334.1	0.27
	Vegetation	282.7	2996.32	199.7	98.82
	Rangeland	3233.4	1508	88578.43	258.86
	Water	3.6	0.31	2.6	278.93

Table 8. Soil erosion and its change from 2000 to 2020

Sub-basin	**Soil erosion tone/he/year**								
	2000	**2020**	**Rate of change**		**Soil erosion 2000**	**Soil erosion in 2020**	**Rate of change**		**average soil erosion relative to the total area in 2000**	**average soil erosion relative to the total area in2020**
			tone	**percent**			**tone**	**percent**		
1	67844.83	71621.07	3776.25	5.57	2566009	2583351	17341.46	0.68	2.39	2.52
2	549463.72	557596.53	8132.81	1.48					19.78	20.08
3	780352.25	783282.85	2930.60	0.38					43.90	44.07
4	384645.18	386656.10	2010.92	0.52					47.17	47.42
5	783703.44	784194.31	490.88	0.06					47.46	47.49

Table 9: Soil erosion rate for each LULC between 2000-2020

LULC	2000	2020	change		Average per hectare in 2000	Average per hectare in 2020
			rate	percent		
Man-made	43811.34	83512.98	39701.63	90.62	22.00	18.01
Vegetation	38994.60	59547.93	20553.33	52.71	11.00	11.86
Rangeland	2482314.90	2438039.77	-44275.10	-1.78	26.75	27.60
Water	864.14	2225.57	1361.44	157.55	3.02	3.49

Table 10: Soil retention in 2000 and 2020

Sub-basin	Soil retention								
	2000	2020	change		Soil retention in 2000	Soil retention in 2020	Change rate(tone)	Average for each hectare in 2000	Average for each hectare in 2020
			tone	percent					
1	100270.88	96494.63	-3776.25	-3.77				3.5	3.39
2	819131.07	810998.26	-8132.81	-0.993	3826649	3809327.66	-17321.45	29.49	29.2
3	1170300.83	1167370.24	-2930.59	-0.25				65.83	65.67
4	566297.93	564287	-2010.92	-0.355				34.29	34.17
6	1168646.28	1168155.4	-490.876	-0.042				143.31	143.25

Table 11: Change of soil retention in each LULC

LULC	2000	2020	change		Average per hectare in 2000	Average per hectare in 2020
			rate	percent		
Man-made	4882.24	11362.97	6480.73	132.74	2.45	2.45
vegetation	95749.3	142737.87	46988.57	49.075	27.01	28.42
Rangeland	3723830.3	365297.1	-70893.2	-1.9	40.13	41.36
Water	158.19	240.83	82.64	52.24	0.55	0.378

Table 12: Correlation between various factors and soil retention service

Factor	Soil retention service	
	R	Coefficient
Rain Erosivity	83.17	69.18
Elevation	-95.1	90.49
Soil erodibility	90.6	82.21
Land management factor	92.58	85.72
Slope (degree)	95.53	91.27